Basalt Fibre Laminates Non-Destructively Inspected After Low-Velocity Impacts

S Sfarra[1*], **C Ibarra-Castanedo**[2], **F Sarasini**[3], **C Santulli**[4] and

XPV Maldague[2]

[1]Las.E.R. Laboratory, Department of Industrial and Information Engineering and Economics, University of L'Aquila, Piazzale E. Pontieri 1, 67100, Monteluco di Roio - L'Aquila, Italy, +39.0862.434362, *stefano.sfarra@univaq.it

[2]Computer Vision and System Laboratory, Department of Electrical and Computer Engineering, Laval University, 1065, av. de la Médecine, G1V 0A6, Quebec City, Canada

[3]Department of Chemical Engineering Materials Environment, Sapienza-Università di Roma, Via Eudossiana 18, 00184, Rome, Italy

[4]School of Architecture and Design, University of Camerino, Viale della Rimembranza, 63100, Ascoli Piceno, Italy

ABSTRACT

In this work, the use of advanced thermographic techniques for the post-impact defect detection in basalt fibre reinforced composite laminates was investigated. The laminates were previously impacted at different energies, namely 7.5, 15 and 22.5 J and then subjected to accelerated environmental aging or to a coating process in order to conceal the previous damage due to low velocity impact. In both cases the defects could be identified using infrared thermography in the mid-wave infrared (MWIR) spectrum even after the treatments. In addition, short-wave infrared (SWIR) results were employed with the aim to clearly identify unsuspected resin-rich areas. Therefore, the non-thermal part of the infrared spectrum (SWIR) can be coupled with the thermal part (MWIR) providing a complete infrared vision beyond what is perceptible to the naked eye, *i.e.*, in the visible spectrum.

Keywords: Low-velocity impact; Basalt fibres; Infrared thermography; Damage detection; Environmental aging.

1 INTRODUCTION

Environmental concerns have recently stimulated an intense research on the use of natural fibres (*i.e.*, animal, vegetable or mineral) for polymer reinforcement. A great number of vegetable fibres have been investigated[1] with acceptable mechanical properties and low cost, however, they generally suffer from moisture sensitivity and low adhesion to hydrophobic polymer matrices. Among natural materials, basalt, which is found in volcanic rocks originated from frozen lava with a melting temperature between 1500 °C and 1700 °C, has received increasing attention not only for the reinforcement of polymers[2,3], but also for metals[4] and ceramics[5,6] due to its advantages in terms of mechanical properties, sound insulation properties, low water absorption, good resistance to chemical attack, high operating temperature range, low environmental impact and lack of carcinogens and health hazards. Despite this plethora of potential applications, the use of basalt fibres has been restricted in the last decades mainly to the reinforcement of both, thermoset and thermoplastic polymers, with a view to possibly replacing its competitor, *i.e.*, glass fibres. In the field of polymer matrix composites, a major threat is represented by low velocity impact because such loading by foreign objects during composite structures life may occur during the phase of manufacturing, maintenance, and operation. The internal damage produced by impact loads can largely affect

their residual mechanical properties even when barely visible impact damage is produced with delaminations and back-face splitting, able to reduce the residual strength by as much as 60%. The purpose of the present work is to extend the thermographic campaign reported in[7] to laminates impacted at different energy levels and subjected to environmental aging highlighting the role of advanced techniques, such as the correlation coefficients and the higher order statistics thermography, in the analysis of raw thermal images in order to enhance the visualization of sub-superficial defects caused by an impact event, even in the case of an applied coating.

2 EXPERIMENTAL

2.1 Materials and low-velocity impact tests

The plain weave basalt fabric (BAS 220.1270.P) was supplied by Basaltex-Flocart NV with a surface weight of 220 g/m^2. The matrix used was a vinylester resin (DION 9102) by Reichhold, Inc, whilst the hardener and accelerator were Butanox LPT (MEKP, 2 wt.%) and NL-51P (Cobalt 2-ethylhexanoate,1 wt.%), respectively. The laminates were manufactured by Resin Transfer Moulding with a fibre volume fraction equal to 0.38 ± 0.02 and a thickness of 3 ± 0.1 mm. From the laminates 100 mm-side square plates were removed for falling weight impact damage characterization using a drop-weight impact tower fitted with an anti-rebound device. A hemispherical impactor with a 12.7 mm diameter tip was used and the samples were clamped to a square frame with a 73 mm square window. Three different impact energies were used in this study, being equal to 7.5, 15 and 22.5 J, respectively.

2.2 Higher Order Statistics Thermography (HOST)

In this work, the performance of the fourth order statistic parameter (*i.e.*, Kurtosis) applied to a pulsed thermography inspection has been explored. The Kurtosis parameter has been used with synthetically generated data processing and they show enhanced defect contrast relative to unprocessed data and high compressing capabilities since the information contained in the unprocessed data sequence is compressed to a unique final image. Kurtosis is generally defined as a measure reflecting the degree to which a distribution is peaked. In particular, Kurtosis provides information regarding the height of the distribution relative to the value of its standard deviation. Mathematically, it is given by:

$$K = \frac{E\left[\left(X - E\left[X\right]\right)^4\right]}{\sigma^4} \tag{1}$$

where, E is the mathematical expectation and σ is the standard deviation. The Kurtosis value can be classified in three general categories according to its deviation from a normal distribution: mesokurtic (normal distribution), leptokurtic (high degree of peakedness) and platykurtic (low degree of peakedness)[8].

The surface temperature evolution for a non-defective area after pulsed thermography testing follows a leptokurtic distribution, where room temperature presents the highest frequency. The Kurtosis value in this case is very high. For a defective zone the surface temperature will present a higher or lower ambient temperature value, depending on the defective material diffusivity. For a defect having a higher thermal diffusivity than the host material, the distribution is more peaked and the kurtosis value is higher for a defective pixel than for a non-defective pixel. In contrast, the distribution has a wider peak and the Kurtosis value is lower for a defective pixel than for a sound pixel for a defective material having a lower thermal diffusivity than the host material. Through this idea, it is possible to estimate the kurtosis values for every pixel in the thermogram matrix and to obtain an image with these values, a kurtogram. The

kurtogram will provide at first an indication of the location of eventual subsurface defects and secondly their thermal diffusivity[9].

2.3 Correlation thermography

The coefficient of linear thermal expansion (CTE) is a material property that is indicative of the extent to which a material expands upon heating. Different substances expand by different amounts when exposed to a thermal front, therefore, the defects inside a composite materials such as resin-rich areas, voids, inclusions, etc., expand autonomously. The correlation coefficients are a solution to characterize the linearity between two signals. In the thermographic context, correlation involves two variables, *i.e.*, the reference and the variable to be compared with it. The latter was computed from a semi-infinite body by referring to the initial temperature of any point of the first thermal image of the sequence, in the same way is done during the differentiated absolute thermal contrast (DAC) computation[10,11]. The image of the body could be represented by a discrete function: value between 0 and 255 of its grey levels. The correlation calculations are done for a group of pixels called pattern. The initial image representing the laminate before displacement is a discrete function *f(x,y)* that will be transformed in another discrete function *f*(x*,y*)* after displacement. The usual correlation coefficients for a correlation technique are obtained as the least square, *i.e.*:

$$C_1 = \int_{\Delta M} \left(f(x,y) - f^*\left(x^*, y^*\right)\right)^2 \cdot dx \cdot dy \qquad (2)$$

where, ΔM represents the surface of the pattern in the initial thermal image[12].

The HOST and correlation thermography techniques have been applied to the thermal infrared vision data, also known as infrared thermographic data[13], while the following techniques, *i.e.*, the Short Wave Infrared Reflectography (SWIR) and Transmittography (WSIRT) have been used for a part of the non-thermal infrared vision data, namely, for a set of acquisitions performed into the short wave infrared spectrum.

2.4 Short Wave Infrared Reflectography (SWIRR) and Transmittography (SWIRT)

Readers can consult[14] in order to acquire a basic knowledge of the techniques applied herein. It is also demonstrated that the speckle pattern shearing interferometry technique[15,16] coherently integrates the non-thermal infrared vision results, in the event that a semi-transparent material becomes a non-transparent material due to a coating process through the application of acrylic paint by spraying.

3 RESULTS AND DISCUSSION

The thermographic acquisition was carried out using an FPA infrared camera (Santa Barbara focal plane SBF125, 3–5 µm) on a 320 by 256-pixel array. The acquisition frequency used was set at 45 Hz. Two high-power flashes (Balcar FX 60), giving 6.4 kJ each for a ~15 ms pulse, were used as heating sources by providing a pulsed stimulation. Data were acquired in reflection mode and processed in Matlab® environment. On the other hand, the non-thermal data were acquired through a SWIR camera (Goodrich SU640SDWH-1.7 RT 640x512 pixels, InGaAs) and an incandescent light bulb, which delivered wide spectrum IR radiation. The radiation source was combined with narrow-band filters in order to limit radiation to the wavelength of interest. The camera and the bulb were placed at approximately the same distance during the acquisitions in reflection and transmission mode.

Although the single use of a SWIRR acquisition (Fig. 1a) does not add anything to the human perception, the use of the digital subtraction of images recorded in reflection and transmission mode (Fig. 1b) points out the fibre misalignment effect caused by an impact event and especially some unexpected resin-rich areas on the upper part of the sample, probably coming from the manufacturing phase. The subsequent application of the distance transform (DT) (Fig. 1c) revealed the widening of the fibres due to the impact loadings, with respect to the normal weave; the misalignment played an important role in the crossing of the light provided by the incandescent bulb. The resin-rich areas were also confirmed by working into the MWIR spectrum, through the use of the advanced techniques explained in the previous section (Figs. 1d-e). In addition, taking advantage of the different thermal conduction between resin rich or starved areas, the thermographic method was able to detect the latter defect on the right side of the sample, delimited by an irregular dotted line. A slight optical (and not thermal) imprint can also be retraced also in Fig. 1b.

FIGURE 1

Quite dissimilar is the case of the laminate impacted at 15 J (Fig. 2a) in which the SWIRR acquisition at 940 nm slightly reveals the presence of an intriguing area around the impact damage. Indeed, after the impact event, the laminate was subjected to an accelerated aging in an environmental chamber (ACS Angelantoni) operating in inert atmosphere. The environmental aging stage followed a cycle of three hours which is schematically reported in Figure 2b. During this cycle, the internal temperature of the chamber was increased of 1 - 2 °C/min up to a plateau temperature (+ 150 °C). After this step, the internal temperature of the chamber was lowered with a cooling rate of 1-2 °C/min up to a minimum temperature (– 70 °C). Each complete sub loading lasted one hour, for a total of three sub loadings which completed the cycle. At the end of the process, the laminate was at first inspected via subtraction of images and after the DT was applied (Fig. 2c) as in the previous case.

FIGURE 2

The result obtained is surprising, since a large delaminated area can now be completely observed. It is also very interesting to notice the fact that the weaker zones, which appear white, now surround the detachment. The presence of the impact zone seems to be lost by working with the SWIRR spectrum. However, the extension of the delaminated area indicated as A in Fig. 2d, can be quantitatively estimated by using the Canny edge operator (Fig. 2d). An area of approximately 3969 mm^2 for a total of 10000 mm^2 can be considered as damaged after the treatment of the laminate inside the environmental chamber, although diffuse resin-starved areas around the large detachment can be observed in the correlation result (Fig. 2e). Both the latter result and the Kurtogram (Fig. 2f) visualize the delaminated area along with the impact zone.

Another optical barrier for the defect retrieval through the SWIRR technique is the application of a coating of acrylic paint (Fig. 3a).

FIGURE 3

The reason is well known in the cultural heritage field, and the explanation was provided by the Kubelka-Munk theory of reflectance[17]. In order to intensify the action of the non-thermal infrared part in the direction of the thermal infrared part, a suitable band working at 1650 nm has been selected. It was also used during the digital image subtraction between the reflectogram and the transmittogram (Fig. 3b) pointing out an unexpected extension of the impact zone marked by an arrow. The optical barrier provided by the acrylic paint covered the fibre misalignment defect also after the application of the DT (Fig. 3c). In practice, the vaporization

effect of the spray acted in order to fill in the interstices between the fibres by varnish. The result is a dark image that doesn't exactly describe the real effect caused by the impact loading at 22.5 J, *i.e.*, three times higher if compared to the case of Fig. 1. Instead, the contribution of the advanced thermographic techniques (Figs. 3d-e) was devoted to: a) the retrieval of the cross shaped damage (Fig. 1a and Fig. 2a) caused by the impact loading, b) the retrieval of a part of the mechanical dent left by the hemispherical tip of the indenter, which appears in reverse colour among the results (*i.e.*, white in the correlation and dark in the Kurtogram), and c) some weaker zones around the holes of the laminate.

In this case, the sub-superficial damage covered by the paint was also confirmed by using the speckle pattern shearing interferometry technique, by considering the distinctiveness of the treatment over a face of the laminate made by basalt fibres. In order to fulfil this task, the thermal load was provided by using a 250 W IR lamp (OSRAM Siccatherm); in addition, a laser with a fundamental wavelength working at 532 nm, vertical polarization and specified power of 250 mW was used in order to create the speckle pattern on the front face of the laminate, obviously randomly distributed in space. Diffusely scattered light from the laminate passed through the halves of a Fresnel biprism of small angles and was focused on the photosensor of a CMOS camera (Canon 40DH 22.2x14.8 mm – 10 megapixel). The two laterally sheared wave fronts interfered each other onto the CCD. In order to measure the surface displacement, a reference speckle pattern (relative to the initial state of the object) was stored. Subsequent specklegrams were subtracted from the reference pattern to obtain the final fringe pattern depicting the slope of the normal displacement. The variation in temperature was monitored by a FLIR S65 HS (7.5–13 μm, 320 x 240 pixels array) thermal camera, that registered a ΔT ~9 °C with respect to the ambient temperature. The heating phase lasted 50 seconds.

Fig. 4 shows the resulting phase map (proportional to the strain distribution) codified in false colours (Fig. 4d) that passes through the addition of carrier fringes (Fig. 4b) in order to work with the phase (Fig. 4c) thanks to the use of the fast Fourier transform (FFT) implemented in Matlab® computer program. It is very interesting to notice that this optical technique was able to retrieve the impact damage partially covered by a layer of acrylic paint (Fig. 4a), as well as the non-perfect round shape left by the falling object, whose unexpected sub-superficial defect is signaled by an arrow in Fig. 4d and already confirmed in Fig. 3b.

FIGURE 4

4 CONCLUSIONS

The work clarifies the key role of the infrared thermography method in the inspection of composite materials. It also tends to underline the importance of the application of advanced techniques, such as the correlation coefficients and higher order statistics thermography, to the raw thermal images in order to enhance the visualization of the shape of sub-superficial defects created by an impact loading. The thermographic method was also able to retrieve the shape and dimensions of the damaged area caused by accelerated aging on previously impact damaged specimens, as well as after a coating treatment by acrylic paint. The mutual interaction between the selected techniques was suitable to improve the visibility of additional details caused or not caused by the impacts. In case of not adhesion between the layers, as shown in Fig. 2, or in case of a material's non-transparency, as illustrated in Fig. 3, the validity of the subtraction between images (*i.e.*, the reflectogram and the transmittogram) loses its importance, as a proper image to be used as an input for the DT was seriously conditioned by the events happened after the impacts. Instead, in the case of the laminate impacted at 7.5 J, the validity of the method was preserved; indeed, the weaker zones arisen after the impacts encircled the damage by following the classical configuration already described in[18].

The speckle pattern shearing interferometry technique was able to retrieve the mechanical imprint due to the tip of the indenter, and the subsequent satellite defect[19] also detected by the method of subtraction of images.

Finally, it was possible to quantitatively estimate the detachment due to the accelerated aging process (Fig. 2), that worked at +100 °C / –70 °C during three complete cycles, thanks to the use of the Canny edge detector implemented into a Matlab® script written *ad hoc* in order to satisfy the purpose[20].

5 ACKNOWLEDGMENTS

The authors would like to thank Eng. Marco Ivagnes and Mr. Fausto Lucantonio (Thales Alenia Space S.p.A. – branch of L'Aquila, Italy) for their kind support during the accelerated aging measurements, as well as Eng. Stefano Perilli (Las.E.R. Laboratory – University of L'Aquila, Italy) for the aid provided during the speckle acquisitions.

6 REFERENCES

[1] M.A. Fuqua, S. Huoa, C.A. Ulven, Natural Fiber Reinforced Composites, POLYM REV 2012, **52**, 259-320, doi: 10.1080/15583724.2012.705409.

[2+ V. Fiore, T. Scalici, G. Di Bella, A. Valenza, A review on basalt fibre and its composites, COMPOS PART B-ENG 2015, **74**, 74–94, doi:10.1016/j.compositesb.2014.12.034.

[3] V. Dhand, G. Mittal, K.Y. Rhee, S.-J. Park, D. Hui, A short review on basalt fiber reinforced polymer composites, COMPOS PART B-ENG 2015, **73**, 166–180, doi: 10.1016/j.compositesb.2014.12.011.

[4] F. Akhlaghi, R. Eslami-Farsani, S.M.M. Sabet, Synthesis and characteristics of continuous basalt fibre reinforced aluminum matrix composites. J COMPOS MATER 2013, **47**, 3379-3388, doi: 10.1177/0021998312465765.

[5] J. Sim, C. Park, D.Y. Moon, Characteristics of basalt fiber as a strengthening material for concrete structures, COMPOS PART B-ENG 2005, **36**, 504–512, doi: 10.1016/j.compositesb.2005.02.002.

[6] N. Kabay. Abrasion resistance and fracture energy of concretes with basalt fiber, CONSTR BUILD MATER 2014, **50**, 95–101, doi: 10.1016/j.conbuildmat.2013.09.040.

[7] S. Sfarra, C. Ibarra-Castanedo, C. Santulli, A. Paoletti, D. Paoletti, F. Sarasini, A. Bendada, X. Maldague, Falling weight impacted glass and basalt fibre woven composites inspected using non-destructive techniques, COMPOS PART B-ENG 2013, **45**, 601–608, doi: 10.1016/j.compositesb.2012.09.078.

[8] R. C. Waugh, "Development of infrared techniques for practical defect identification in bonded joints", Ph.D. Thesis, University of Southampton, 2016.

[9] F.J. Madruga, C. Ibarra-Castanedo, O.M. Conde, X.P. Maldague, J.M. López-Higuera, Enhanced contrast detection of subsurface defects by pulsed infrared thermography based on the fourth order statistic moment, Kurtosis, Proc. SPIE 7299, Thermosense XXXI, San Diego (USA), 2009, doi: 10.1117/12.818684.

[10] M. Susa, H.D. Benítez, C. Ibarra-Castanedo, H. Loaiza, H. Bendada, X. Maldague, Phase contrast using a differentiated absolute contrast method, QIRT J 2006, **3**, 219-230, doi: 10.3166/qirt.3.219-230.

[11] M.T. Klein, C. Ibarra-Castanedo, A. Bendada, X.P. Maldague, Thermographic signal processing through correlation operators in pulsed thermography, Proc. SPIE 6939, Thermosense XXX, Orlando (USA), 2008, doi: 10.1117/12.777002.

[12] T.C. Chu, W.F. Ranson, M.A. Sutton, Applications of digital-image-correlation techniques to experimental mechanics, EXP MECH 1985, **25**, 232-244, doi: 10.1007/BF02325092.

[13] X.P.V. Maldague, Theory and practice of infrared technology for nondestructive testing, John Wiley & Sons, New York, 2001.

[14] A. Bendada, S. Sfarra, M. Genest, D. Paoletti, S. Rott, E. Talmy, C. Ibarra-Castanedo, X.P. Maldague, How to reveal subsurface defects in Kevlar® composite materials after an impact loading using infrared vision and optical NDT techniques?, ENG FRACT MECH 2013, **108**, 195–208, doi: 10.1016/j.engfracmech.2013.02.030.

[15] M. Owner-Petersen, Digital speckle pattern shearing interferometry: limitations and prospects, APPL OPTICS 1991, **30**, 2730–2738, doi:10.1364/AO.30.002730.

[16] S. Sfarra, P. Theodorakeas, N. P. Avdelidis, M. Koui, Thermographic, ultrasonic and optical methods: A new dimension in veneered wood diagnostics, RUSS J NONDESTRUCT+ 2013, **49**, 234-250, doi: 10.1134/S1061830913040062.

[17] W.E. Vargas and G.A. Niklasson, Applicability conditions of the Kubelka-Munk theory, APPL OPTICS 1997, **36**, 5580-5586, doi: 10.1364/AO.36.005580.

[18] S. Sfarra, C. Ibarra-Castanedo, C. Santulli, F. Sarasini, D. Ambrosini, D. Paoletti, X. Maldague, Eco-Friendly Laminates: From the Indentation to Non-Destructive Evaluation by Optical and Infrared Monitoring Techniques, STRAIN 2013, **49**, 175-89, doi: 10.1111/str.12026.

[19] S. Sfarra, C. Ibarra-Castanedo, F. Lambiase, D. Paoletti, A. Di Ilio and X. Maldague, From the experimental simulation to integrated non-destructive analysis by means of optical and infrared techniques: results compared, MEAS SCI TECHNOL 2012, 23, 115601, doi: 10.1088/0957-0233/23/11/115601.

[20] S. Sfarra, F. López, F. Sarasini, J. Tirillò, L. Ferrante, S. Perilli, C. Ibarra-Castanedo, D. Paoletti, L. Lampani, E. Barbero, S. Sánchez-Sáez and X. Maldague, Analysis of damage in hybrid composites subjected to ballistic impacts: an integrated non-destructive approach, in Handbook of Composites from Renewable Materials, edited by V.K. Thakur, M.K. Thakur, M.R. Kessler, Wiley-Scrivener, 2016, in press.

FIGURE CAPTIONS

Figure 1. Laminate impacted at 7.5 J: (a) SWIRR result at 940 nm, (b) Image subtraction between the reflectogram and the transmittogram acquired at 940 nm, (c) Distance Transform (DT) applied on Fig. (b), (d) Correlation result, and (e) Kurtogram

Figure 2. Laminate impacted at 15 J: (a) SWIRR result at 940 nm, (b) Graph inherent to the accelerated aging cycle, (c) Distance Transform (DT) applied on the image subtraction result, (d) Segmentation process after the image subtraction between the reflectogram and the transmittogram acquired at 940 nm, (e) Correlation result, and (f) Kurtogram

Figure 3. Laminate impacted at 22.5 J: (a) SWIRR result at 1650 nm, (b) Image subtraction between the reflectogram and the transmittogram acquired at 1650 nm, (c) Distance Transform (DT) applied on Fig. (b), (d) Correlation result, and (e) Kurtogram

Figure 4. Laminate impacted at 22.5 J: (a) Visible image, (b) Phase image, (c) Phase image processed, and (d) Phase image detail in false colors centred on the impacted zone

FIGURES

Figure 1

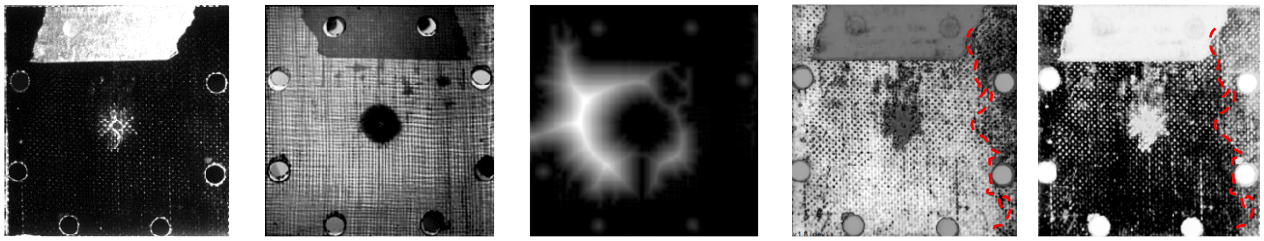

(a) (b) (c) (d) (e)

Figure 2

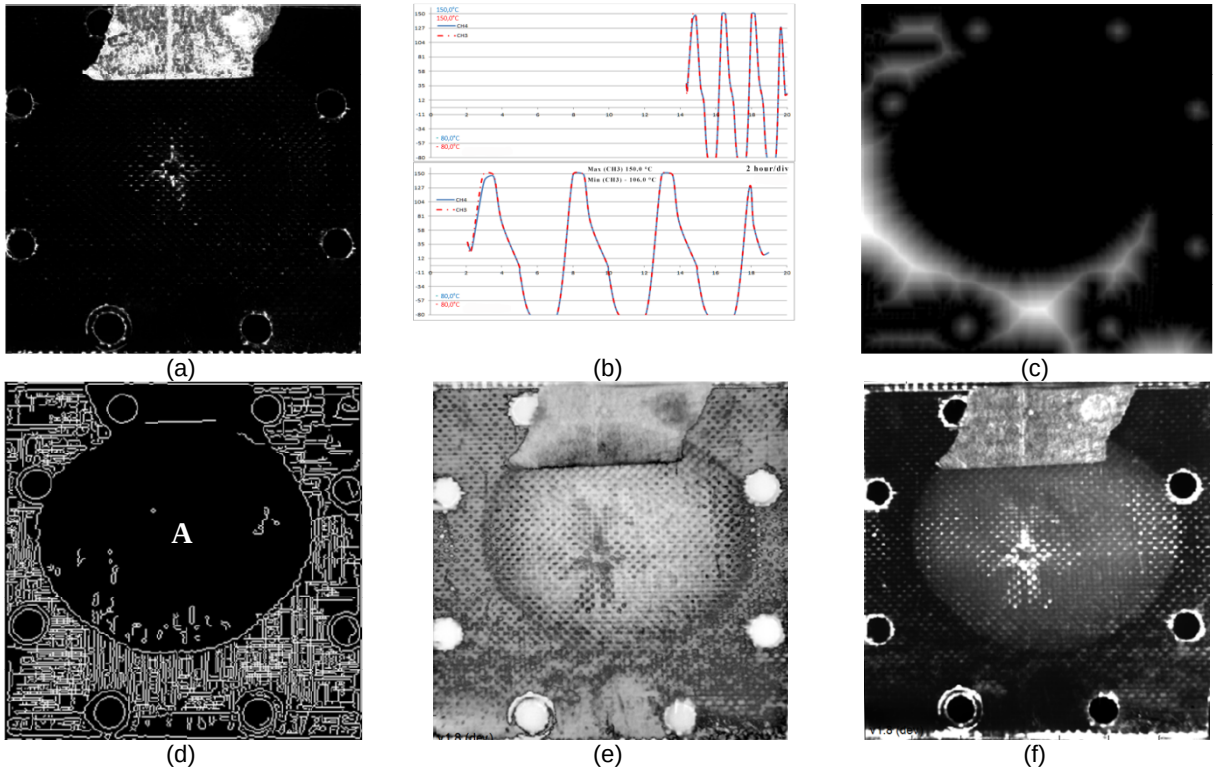

(a) (b) (c)

(d) (e) (f)

Figure 3

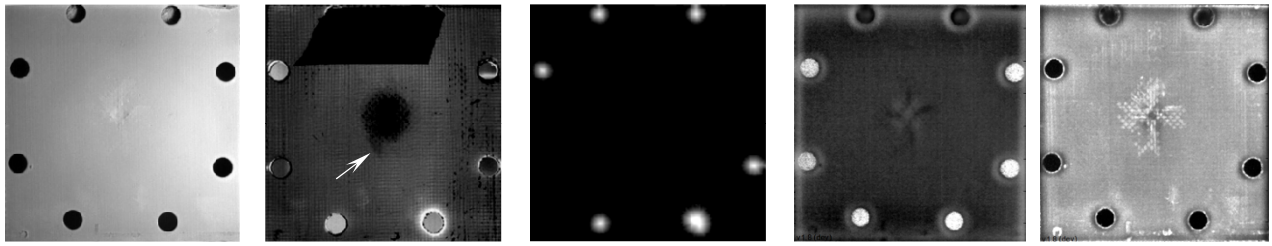

(a) (b) (c) (d) (e)

Figure 4

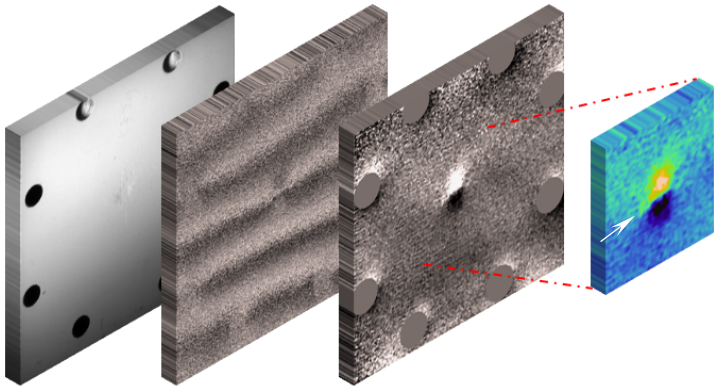

(a) (b) (c) (d)